

Proton-impact-induced electron emission from biologically relevant molecules studied with a screened independent atom model

Hans Jürgen Lüdde*

Frankfurt Institute for Advanced Studies (FIAS), D-60438 Frankfurt, Germany

Marko Horbatsch[†] and Tom Kirchner[‡]

Department of Physics and Astronomy,

York University, Toronto, Ontario M3J 1P3, Canada

(Dated: September 22, 2021)

Abstract

We use the recently introduced independent-atom-model pixel counting method to calculate proton-impact net ionization cross sections for a large class of biologically relevant systems including pyrimidines, purines, amino acids, and nucleotides from 10 keV to 10 MeV impact energy. Overall good agreement with experimental data, where available, is found. A scaling prescription that involves coefficients derived from the independent atom model is shown to represent the cross section results better than scalings based on the number of (bonding) valence electrons of the target molecules. It is shown that the scaled net ionization cross sections of the proton-nucleotide collision systems can be represented in terms of a simple analytical formula with four parameters to within 3% accuracy.

PACS numbers: 34.10.+x, 34.50.Gb, 34.70.+e, 36.40.-c

* luedde@itp.uni-frankfurt.de

† marko@yorku.ca

‡ tomk@yorku.ca

I. INTRODUCTION

There has been growing interest in collisions involving organic compounds and biomolecules in recent years. That interest and the ensuing research activity are largely driven by data needs in areas ranging from astrochemistry to ion-beam cancer therapy. Ideally, the cross section data required, e.g., for a detailed understanding of the radiation damage of biological tissue [1], would be obtained from systematic measurements and first-principles calculations. While progress has been made on both experimental (see [2–9] for proton-impact collisions) and theoretical [10–12] fronts, the complexity and multitude of molecules of interest suggest that there is a role to be played by simplified models which are easily applicable to a wide range of collision systems.

Classical arguments or quantum-mechanical first-order perturbation theory represent natural starting points for modeling electron removal in ion-molecule collisions. Making use of these ingredients, a number of analytical cross section formulae have been proposed and applied (see, e.g., [13–15] and the discussion in [9]). Their advantage is simplicity—typically they only require the binding energies of the target electrons as physical input—but their success depends on (additional) parameters which are determined (semi-) empirically. As a consequence, these analytical models do not have sufficient predictive power, and are thus of limited value for problems for which measurements or more sophisticated calculations are not available.

Most attempts at constructing more sophisticated models are based on the idea that the ionization or capture cross section of a complex molecule may be linearly combined from smaller parts. In the *complete neglect of differential overlap* (CNDO) approach a Mulliken-like population analysis is applied to an electronic structure calculation of the target molecule. The molecular cross section is then written as a linear combination of contributions from all atomic orbitals involved, with the Mulliken populations as weight factors [16]. A related class of models is based on the additivity rule (AR) according to which the ionization or capture cross section for a specific target system is obtained as a sum of cross sections of its building blocks. Normally, atomic building blocks are used and the description is referred to as independent-atom-model (IAM)-AR. In a recent work it was argued that one can also start from small molecular constituents to assemble the ionization cross section of a larger molecule [17]. A caveat of this independent-molecule-model (IMM)-AR is that there are

usually many different ways to decompose a given molecule into molecular building blocks and depending on which ansatz is used the resulting cross section may vary. It should also be noted that the IMM-AR work of [17] used experimental cross section data for the building blocks as input, while the atom-like contributions in the CNDO approach are usually obtained from perturbative collision calculations [16, 18–20].

Motivated by the somewhat limited scope of these models we recently introduced an IAM-based description of ion-molecule collisions which uses first-principles-based atomic cross section calculations and goes beyond the simple AR [21]. The main assumption of our model is that the net ionization and capture cross sections can be represented as *weighted* sums of atomic net cross sections for all the atoms that make up the molecule. The weight factors account for the geometrical overlap which occurs when one projects the loci of the atomic centers of the molecule onto a plane perpendicular to the projectile beam direction and pictures the atomic cross sections as circular disks in that plane. The “visible” effective cross sectional area is calculated using a pixel counting method (PCM) and, accordingly, we refer to the model as IAM-PCM. In the limit of small overlaps the IAM-PCM cross section approaches the result of the IAM-AR. This is a desirable property since the IAM-AR is known to give fairly accurate results in the high-impact-energy regime in which capture and ionization cross sections are small and geometrical overlap is negligible. Toward lower energies, capture and ionization become stronger and the IAM-AR tends to overestimate experimental data [17, 21]. In applications to proton collisions from medium-sized molecules such as H₂O and from larger water, neon, and carbon clusters we have found that geometrical overlap does occur at these lower energies and leads to significant cross-section reductions [21, 22]. Compared to the IAM-AR the agreement with experimental data, where available, is improved.

Given these promising results and the relative simplicity of the model, the IAM-PCM seems ideally suited to study collisions from complex biomolecules for which neither ab-initio calculations nor measured cross section data are available. This is the main objective of the present work. In particular, we examine scaling relations obtained from IAM-PCM calculations for proton-impact net ionization cross sections of different groups of systems such as amino acids and nucleotides, and suggest a parametrization of our results in terms of a simple analytical formula.

The layout of the paper is as follows. We begin in section II with a short summary

of the IAM-PCM. For a more detailed description the reader is referred to [22]. In section III we seek to further validate the model, beyond the results presented in [21, 22], by comparing calculated net ionization cross sections with available measurements and previous theoretical and semi-empirical model data for 10 keV to 10 MeV proton collisions from pyrimidine ($C_4H_4N_2$), purine ($C_5H_4N_4$), tetrahydrofuran (THF – C_4H_8O) and trimethyl phosphate (TMP – $(CH_3)_3PO_4$). Different scaling prescriptions for the net ionization cross section are examined and applied to a large class of systems including amino acids and nucleotides in section IV and a simple parametrization of these results is suggested in section V. The paper ends with concluding remarks in section VI.

II. THEORETICAL MODEL

The ingredients of the IAM-PCM are atomic cross sections and molecular ground-state geometries. The latter are taken from the literature using a Cartesian coordinate representation [23], which is commonly referred to as xyz-file format. More specifically, for the biomolecules studied in this work we use data provided through [24]. The proton-atom net ionization cross sections are calculated in a density functional theory (DFT) framework on the level of the independent electron model. We use a well-tested no-response model in which the Kohn-Sham potential is approximated by an accurate exchange-only ground-state potential [25] and time-dependent screening and exchange effects are neglected. The nonperturbative two-center basis generator method (TC-BGM) is used for orbital propagation [26]. It yields transition probabilities and cross sections for target excitation and electron transfer to the projectile (capture) and the continuum (ionization). In the present work we only look at the ionization channel, since it usually exhibits simpler scaling properties and there are no capture data available for comparison for most of the molecules studied here.

The net ionization cross sections σ_j^{net} for the $j = 1, \dots, N$ atoms that make up the molecule under study are combined according to

$$\sigma_{\text{mol}}^{\text{net}}(E, \alpha, \beta, \gamma) = \sum_{j=1}^N s_j(E, \alpha, \beta, \gamma) \sigma_j^{\text{net}}(E) \quad (1)$$

to yield the molecular cross section at projectile energy E . The weight factors $0 \leq s_j \leq 1$ account for the overlap of the atomic cross sections and depend on the relative orientation of the molecule with respect to the ion beam direction. This dependence is captured by the

Euler angles α, β, γ .

To calculate the weights we picture the atomic cross sections as circular disks with radii $r_j(E) = [\sigma_j^{\text{net}}(E)/\pi]^{1/2}$ in a plane perpendicular to the ion beam axis. The combined area of overlapping circles is broken up into pixels and calculated by counting those pixels that are visible to the impinging projectile. Accordingly, the screening coefficients can be determined by

$$s_j(E, \alpha, \beta, \gamma) = \frac{\sigma_j^{\text{vis}}(E, \alpha, \beta, \gamma)}{\sigma_j^{\text{net}}(E)}, \quad (2)$$

where σ_j^{vis} is the visible part of the j th atomic cross section.

The IAM-PCM is similar in spirit to the so-called screening-corrected additivity rule (SCAR) developed and used for electron-molecule collisions [27]. SCAR cross sections, however, are based on a heuristic recurrence relation for the determination of the screening coefficients in an orientation-independent version of (1), whereas the IAM-PCM procedure to calculate them for any given orientation is numerically exact. In order to compare IAM-PCM calculations with experimental data for *randomly* oriented molecules we repeat the pixel count for an ensemble of Euler angle triples and average the cross-section results appropriately.

Once the atomic cross sections have been calculated, the IAM-PCM procedure is not at all resource intensive. It takes just a few minutes on a single-core computer to carry out an orientation average at a given energy for a system consisting of dozens of nuclei and hundreds of electrons. The reader is referred to [22] for more details.

III. VALIDATION OF THE MODEL

The molecules pyrimidine, purine, THF, and TMP are structural analogues of DNA constituents and have been studied in recent collision experiments [8, 9, 28], since they were deemed more amenable to gas-phase cross-section measurements than actual DNA building blocks¹. More specifically, pyrimidine is a single carbon-nitrogen-ring molecule from which the nucleobases cytosine and thymine (and the RNA nucleobase uracil) are derived, while the double-ring molecule purine is a precursor of the nucleobases adenine and guanine. Both

¹ While it is difficult to prepare well-characterized gas targets of large neutral DNA components, the technique of electrospray ionization offers a pathway to bringing *charged* complex biomolecules into the gas phase and use them in collision experiments [29].

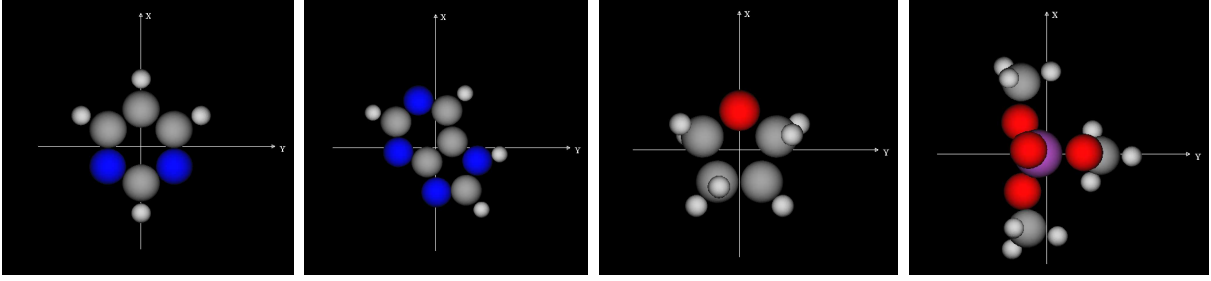


FIG. 1. Net ionization in $E = 500$ keV proton collisions with (from left to right) pyrimidine ($C_4H_4N_2$), purine ($C_5H_4N_4$), THF (C_4H_8O), TMP ($(CH_3)_3PO_4$) for particular orientations. The radii of the circular disks are given by $r_j = [\sigma_j^{\text{net}}/\pi]^{1/2}$ using TC-BGM proton-atom net ionization cross sections σ_j^{net} .

pyrimidine and purine are also used as generic names for wider classes of similar one-ring and two-ring molecules, respectively, which include the DNA and RNA nucleobases (see section IV). THF serves as a model for the monosaccharide deoxyribose in DNA, and TMP represents the phosphate residue which together with the sugar molecule forms the DNA backbone [30, 31].

Figure 1 displays effective cross sectional areas for proton collisions from these four molecules for arbitrary orientations with respect to the projectile beam axis. The atomic nuclei are placed at their equilibrium ground-state positions and the plots are obtained from net ionization calculations at $E = 500$ keV impact energy. For pyrimidine and purine there is no overlap of the atomic cross sections for the chosen geometries, while a modest overlap effect occurs for THF and a somewhat larger one for TMP. One can imagine how the magnitude of the overlap effect varies as a function of orientation and collision energy and that even for pyrimidine, the smallest of the four molecules, the orientation-averaged IAM-PCM cross section will be smaller than the zero-overlap limit corresponding to the IAM-AR.

Figure 2 shows the orientation-averaged net ionization cross section for proton-pyrimidine collisions as a function of impact energy. In the left panel [figure 2(a)], we compare several model calculations on a double-logarithmic scale which emphasizes the fall-off of the ionization cross section toward high impact energy. This shows nicely how the present IAM-AR and IAM-PCM results merge in the $E \geq 1000$ keV range in which the atomic cross sections are so small that no significant overlap occurs for *any* orientation. This is very different at

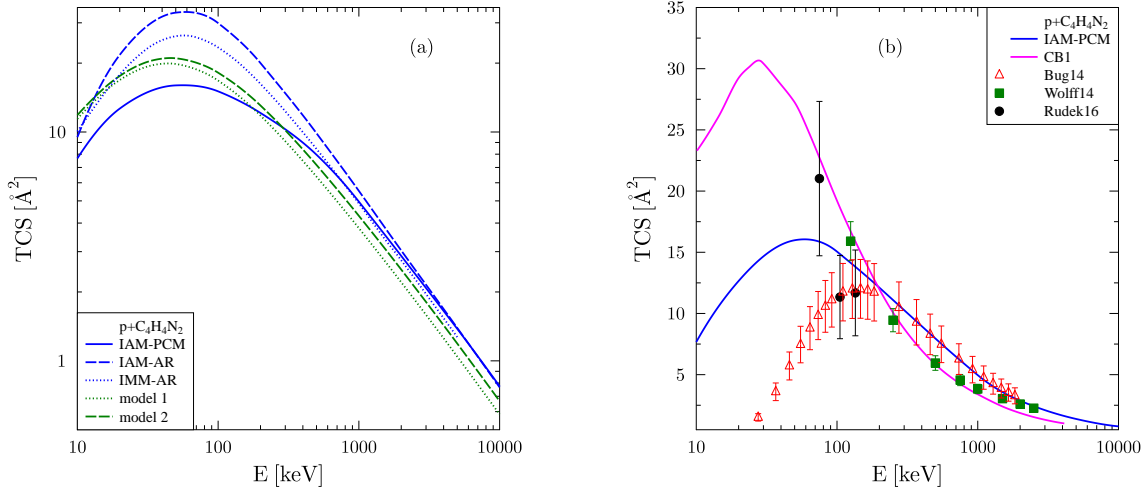


FIG. 2. Total net ionization cross section for proton-pyrimidine ($C_4H_4N_2$) collisions as a function of impact energy on (a) a double-logarithmic scale and (b) a single-logarithmic scale. IAM-PCM, IAM-AR: present calculations, IMM-AR [9], model 1 and model 2 denote model calculations based on equations (3) and (4) as described in the text; CB1: first Born approximation with corrected boundary conditions within the CNDO approach [9]; experiments: Bug14 [32] (see also [28]) for electron impact using equivelocity conversion, Wolff14 [8], Rudek16 [9] for proton impact.

lower energies: At the cross section maximum around $E = 60$ keV the IAM-AR cross section is about a factor of two larger than its IAM-PCM counterpart.

The two IAM calculations bracket the IMM-AR results reported in [9] in most of the impact energy range shown. This is expected based on geometrical considerations. On the one hand the (experimental) molecular cross sections used in the IMM-AR to assemble the cross section for pyrimidine should be smaller than the zero-overlap IAM-AR predictions, but on the other hand their sum should be larger than the IAM-PCM cross section for pyrimidine, since overlaps of the contributing molecular cross sections are neglected in the IMM-AR. The fact that the IMM-AR results become slightly smaller than the IAM-PCM calculations above $E = 1000$ keV cannot be explained on geometrical grounds. It points either to an underestimation of the overlap effect by the IAM-PCM or to a small inconsistency between the (atomic) TC-BGM results and the experimental cross section data used in the IMM-AR

calculation of [9]. Given that no details about the latter were provided, we cannot offer a more definitive explanation for the (small) discrepancy.

The two model calculations included in figure 2(a) are based on a semi-empirical scaling relation proposed by Montenegro and co-workers [15], and used for proton-pyrimidine collisions in [8]. According to that model the net ionization cross section of an atom or molecule can be written as

$$\sigma^{\text{net}}(E) = \sum_k \sigma_k(E) = \sum_k \frac{Z_k \delta_k}{I_k^2} F\left(\frac{E/M}{I_k}\right) \quad (3)$$

with the universal function

$$F(x) = \frac{A \ln(1 + Bx)}{x} - \frac{AB}{(1 + Cx)^4}. \quad (4)$$

The sum in (3) is over the contributing atomic or molecular orbitals, Z_k is the occupation number and I_k the ionization potential (in atomic units) of the k th orbital, δ_k a parameter, and E/M the collision energy in keV/amu. The universal parameters in (4) are $A = 6.15 \times 10^3$, $B = 7.0 \times 10^{-2}$, and $C = 1.4 \times 10^{-2}$ to yield cross sections measured in units of 10^{-18} cm² [15].

The model 1 calculation is identical to that reported in [8]. It uses the ionization potentials of the eleven most loosely bound, doubly-occupied ($Z_k = 2$) orbitals of pyrimidine quoted in [8] and $\delta_k = 0.66$ for all k . For model 2 we make the same choices for Z_k and δ_k , but use the ionization potentials of the fifteen valence orbitals provided in [9], which are slightly different from those quoted in [8] for the outermost eleven. Both model variants lead to similarly shaped cross section curves with the model 2 results being larger than the model 1 results by 12–14 % in the $E = 300$ keV to $E = 10$ MeV range in which the curves appear as almost perfect straight lines on the double-logarithmic plot. The difference in magnitude is mostly due to the fact that four additional orbitals are taken into account in model 2.

We also carried out a model calculation based on the fifteen most loosely bound *atomic* orbitals using the exchange-only DFT orbital energy eigenvalues on which the TC-BGM calculations are based. Given that the high-energy behavior of the model cross section is controlled by the first, Bethe-Born-like, term in equation (4) and the TC-BGM has been shown to give results which agree very well with Bethe-Born predictions at high energies (see section V and [22]), one would expect that this model variant would agree with the IAM-PCM calculations at least in the high-energy limit. However, we found that the results of the atomic model are very similar to those of model 2 (which is why they are not included

in the figure) and, as a consequence, somewhat smaller than the IAM-PCM cross section at $E \geq 300$ keV. We have checked that the high-energy discrepancy would essentially be eliminated if one would use $\delta_k = 1.0$ instead of $\delta_k = 0.66$ in the model. Such a choice would be consistent with the findings of [15]: In that paper $\delta = 0.66$ was used to describe p-H collisions, while $\delta = 1.0$ was found to give excellent fits of the experimental ionization cross sections in the p-N₂ and p-CH₄ systems. But even such an amended model would not agree with the IAM-PCM results at lower impact energies, i.e., the latter are incompatible with equations (3) and (4). This suggests that in general one cannot expect very accurate results when applying these equations to collisions involving complex biomolecules.

Figure. 2(b) displays on a single-logarithmic plot the IAM-PCM results together with experimental data for proton [8, 9] and equivelocity electron impact [32] and the results of a first Born calculation with corrected boundary conditions (CB1) performed within the CNDO approach [9]. The CB1 calculation gives smaller cross section values than the IAM-PCM at energies above $E = 200$ keV, in apparent agreement with most of the experimental data points of [8]. However, the CB1 and experimental results differ in energy dependence above $E = 1000$ keV. This is better seen on the double-logarithmic plot provided in figure 5(a) of [9]. The IAM-PCM results agree very well with the electron-impact measurements of [32] in the region above the cross section maximum in which electron-impact data are expected to approach the proton-impact cross section. Indeed, within combined error bars the electron-impact data are in marginal agreement with the proton measurements of [8], although it appears as if the latter fall somewhat below the former. New experimental data with smaller error bars would be needed to draw more definitive conclusions about the high-energy behavior of the cross section.

The three experimental proton-impact data points of [9] at intermediate energies have too large uncertainties to help shed light on the increasing deviations between the CB1 and IAM-PCM calculations in this region. Given the first-order nature of the CB1 one would not expect this model to be valid below $E = 100$ keV, but in the absence of more experimental data the overall situation remains unclear.

Figure 3 shows IAM-PCM net ionization cross section results for proton-purine collisions. We compare them with equivelocity electron-impact measurements from [32] only, since we are not aware of other theoretical calculations or measurements for proton impact. Consistent with the pyrimidine case, the agreement is excellent in the energy region above the

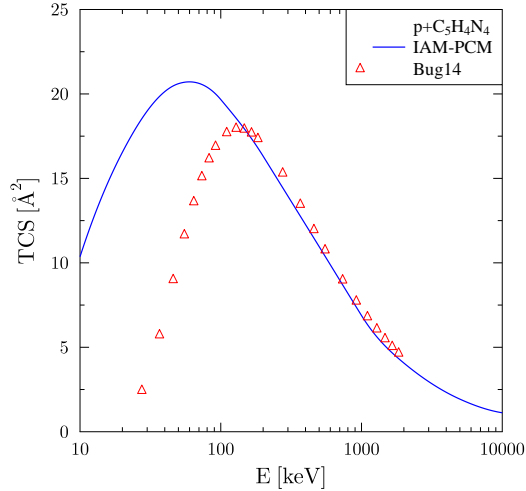


FIG. 3. Total net ionization cross section for proton-purine ($C_5H_4N_4$) collisions as a function of impact energy. IAM-PCM: present calculation; experiments: Bug14 [32] (see also [28]) for electron impact using equivelocity conversion.

experimental cross section maximum in which the sign of the projectile charge is deemed to be unimportant.

Similar observations are made for the THF and TMP target molecules, as shown in figures 4 and 5, respectively. For these two cases, in addition to the electron data from [32], proton-impact cross section measurements and CB1 calculations from [9] are available for comparison. As for the proton-pyrimidine case, the CB1 results are somewhat lower than the IAM-PCM cross sections at relatively high impact energies where first-order perturbation theory is expected to be valid. They cross the IAM-PCM curve between $E = 100$ and $E = 200$ keV and are probably too high at lower energies where the perturbation is too strong for a first-order theory to be reliable. The measured data points of [9] appear somewhat unsystematic and have error bars that are too large to differentiate between the CB1 and IAM-PCM calculations. At high energies in particular, new measurements with smaller uncertainties are highly desirable to clarify the situation. This caveat notwithstanding, the IAM-PCM results appear to agree with most experimental data points for the four collision systems studied in this section. We thus feel encouraged to expand the application of the model to a larger class of systems for which experimental data are sparse and theoretical predictions are required.

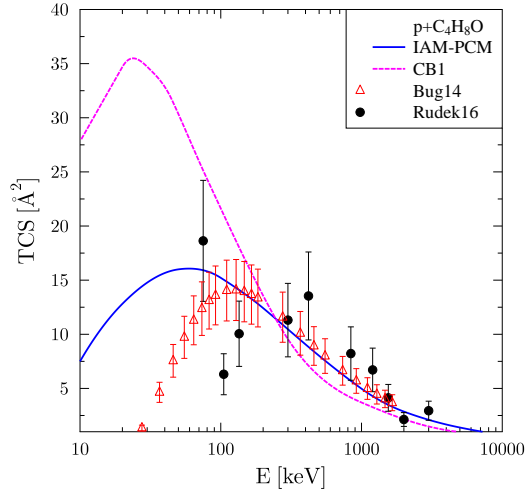


FIG. 4. Total net ionization cross section for p-THF (C_4H_8O) collisions as a function of impact energy. IAM-PCM: present calculation, CB1: first Born approximation with corrected boundary conditions within CNDO approach [9]; experiments: Bug14 [32] (see also [28]) for electron impact using equivelocity conversion, Rudek16 [9] for proton impact.

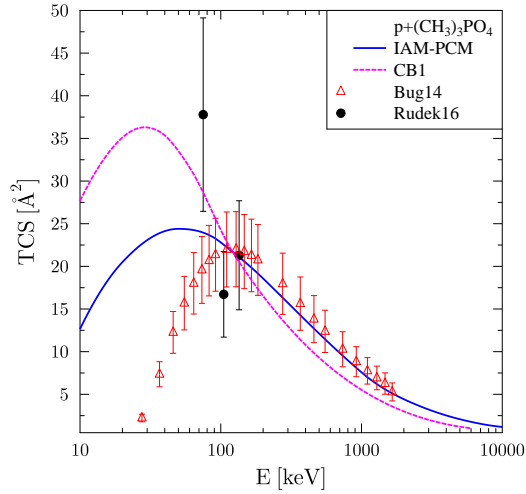


FIG. 5. Total net ionization cross section for p-TMP ($(CH_3)_3PO_4$) collisions as a function of impact energy. IAM-PCM: present calculation, CB1: first Born approximation with corrected boundary conditions within CNDO approach [9]; experiments: Bug14 [32] (see also [28]) for electron impact using equivelocity conversion, Rudek16 [9] for proton impact.

IV. SCALING PROPERTIES

Previous experimental and theoretical work provided some evidence that the (total) proton-impact electron emission cross sections of large biomolecules scale with the number of valence electrons [5, 9, 17, 28]. However, only a relatively small set of molecules has been investigated so far and it is not clear whether the observed approximate scaling applies to a larger class of systems and can be used to predict cross sections for experimentally inaccessible compounds. In this section we investigate this question by using the IAM-PCM to calculate proton-impact net ionization cross sections for four groups of biologically relevant systems: pyrimidines, purines, amino acids, and nucleotides, the latter constituting the monomeric units of RNA and DNA [30, 31]. To our knowledge, for most of the studied species the results presented here are the first cross section data obtained from systematic, parameter-free calculations. Exceptions are the five DNA/RNA nucleobases cytosine, thymine, uracil, adenine and guanine. As mentioned in section III the first three fall into the category of pyrimidines, while the latter two are purines. For all of them classical [33, 34] and perturbative [35] cross section calculations have been carried out, the latter in some cases within the CNDO approach [16, 18, 20]. A comparison with those earlier calculations, the IMM predictions of [17], and the limited experimental data available [4–7] will be presented elsewhere [36].

In the following, we consider three different scaling prescriptions. The first one uses the standard textbook definition of valence electrons according to which all electrons in the outermost n -shells of the atoms that form the molecule under study are included in the valence-electron count [37]. In the second variant we only count the *bonding* valence electrons, i.e., those electrons that form *lone pairs* are excluded. The scaled cross section is obtained by dividing the orientation-averaged IAM-PCM result for a molecule with formula $C_{n_1}H_{n_2}N_{n_3}O_{n_4}P_{n_5}$ by the numbers

$$N_{\text{VE}} = 4n_1 + n_2 + 5n_3 + 6n_4 + 5n_5 \tag{5}$$

and

$$N_{\text{BVE}} = 4n_1 + n_2 + 3n_3 + 2n_4 + 5n_5, \tag{6}$$

respectively, assuming in the latter case that all L -shell electrons of carbon participate in bonds (through hybridization), while in nitrogen one and in oxygen two electron pairs do

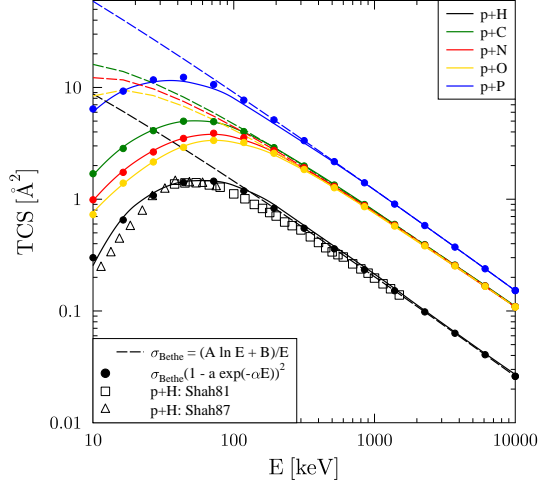


FIG. 6. Total net ionization cross sections for proton collisions with atomic hydrogen (H), carbon (C), nitrogen (N), oxygen (O), and phosphorus (P) as functions of impact energy. Full lines: present TC-BGM calculations, dashed lines: Bethe-Born ionization cross sections $\sigma_{\text{Bethe}} = (A \ln E + B)/E$ with fit parameters A and B in appropriate units (see section V), (\bullet): parametrizations discussed in section V. Experiments for p-H: Shah81 [38], Shah87 [39].

not.

The third prescription is based on the IAM and the observation that at high impact energies the net ionization cross sections for p-C, p-N, and p-O collisions are very similar (i.e., $\sigma_X^{\text{net}} \equiv \sigma_C^{\text{net}} \approx \sigma_N^{\text{net}} \approx \sigma_O^{\text{net}}$) and to a good approximation four times larger than the p-H cross section [22]. This is demonstrated in figure 6, where the corresponding TC-BGM results are shown. Since the nucleotides studied further below contain phosphorus, the p-P collision system is included in figure 6 as well. In this case, we find that the net ionization cross section is approximately 1.5 times as large as that for carbon, nitrogen, and oxygen. Accordingly, the high-energy IAM prediction for the net ionization cross section of the molecule $C_{n_1}H_{n_2}N_{n_3}O_{n_4}P_{n_5}$ is to a good approximation $(n_1 + n_2/4 + n_3 + n_4 + 3n_5/2)\sigma_X^{\text{net}}$, and we scale the (orientation-averaged) IAM-PCM cross sections in this variant by dividing them by the (fractional) coefficients

$$N_{\text{IAM}} = n_1 + \frac{n_2}{4} + n_3 + n_4 + \frac{3n_5}{2}. \quad (7)$$

Figure 7 displays the scaled and unscaled cross section results for all systems studied in

this section. The unscaled IAM-PCM cross sections are also provided in tabulated form in the Appendix. For the pyrimidines [figure 7(a)] and purines [figure 7(b)] the scaling with respect to the number of bonding valence electrons yields better results than that with respect to the number of all valence electrons. For the amino acids [figure 7(c)] the situation is reversed, most visibly so in the region around the cross section maximum, while for the nucleotides [figure 7(d)] both scaling procedures appear to work equally well.

A more conclusive picture emerges when the cross sections are scaled by dividing them by the fractional IAM coefficients (7). In this case, we obtain for each group of systems a nearly universal curve. Given the atomic results shown in figure 6 this is to be expected at high energies where the IAM-PCM cross sections approach the IAM-AR limit. However, it is not obvious that the scaling should also hold at lower energies where significant atomic cross section overlaps occur and the IAM-PCM calculations are not orientation independent; e.g., we found that at $E = 100$ keV the net ionization cross section of pyrimidine varies within a factor of two as a function of orientation. It is one of the main results of this work that despite these caveats the scaling holds if one accepts tolerances on the order of 10%.

Figure 8 provides a more differentiated view of the approximate universality of the IAM-based scaling. It shows on a linear scale averages of the IAM-normalized cross sections and the deviations from these averages as error bars. For the pyrimidines these deviations are as large as $\sim \pm 10\%$, while for the DNA nucleotides they are smaller than $\pm 2\%$. The negligible spread of the latter can be traced back to the sugar-phosphate backbone, which is the same for all DNA nucleotides, and, due to the large p-P cross section (cf. figure 6), is the main contributor to the total cross section. Our results then indicate that the differences in the cross sections of the pyrimidines and purines are not relevant for the ionization of a DNA molecule. Rather, they suggest that one can understand the latter as the ionization of one or another of its nucleotide monomers, all of which fulfill the IAM-based scaling relation very accurately, i.e., it does not matter much which of them is actually ionized.

V. PARAMETRIZATION

The finding that the IAM-based scaling works very well for a large class of systems raises the question whether the proton-impact electron emission cross sections of biomolecules can be parametrized in a convenient way. To address this question we re-inspect figure 6 which in

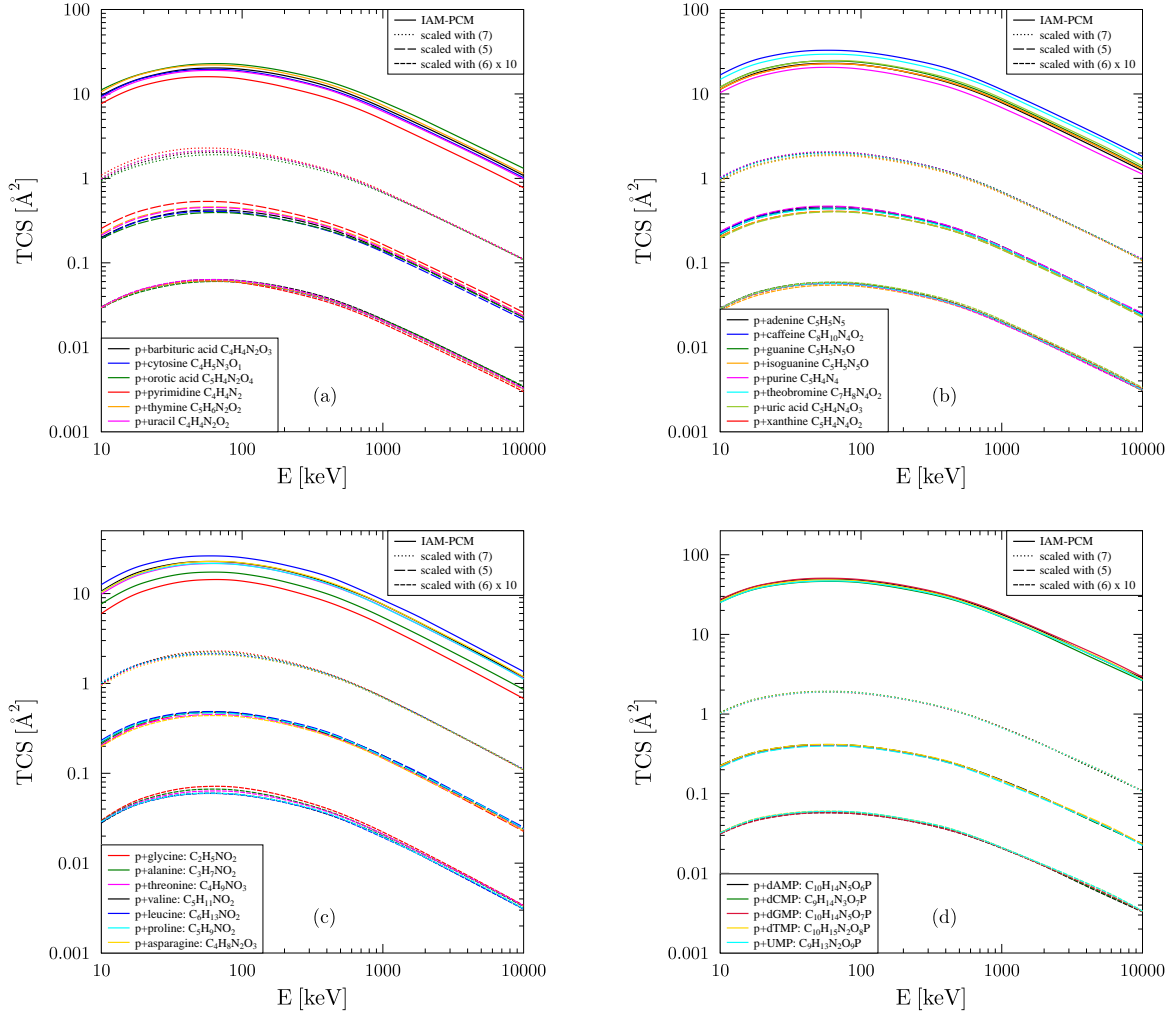


FIG. 7. Total net ionization cross sections for proton collisions with (a) the pyrimidines barbituric acid, cytosine, orotic acid, pyrimidine, thymine, uracil; (b) the purines adenine, caffeine, guanine, isoguanine, purine, theobromine, uric acid, xanthine; (c) the amino acids glycine, alanine, threonine, valine, leucine, proline, asparagine; (d) the DNA nucleotides deoxyadenosine monophosphate (dAMP), deoxycytidine monophosphate (dCMP), deoxyguanosine monophosphate (dGMP), deoxythymidine monophosphate (dTMP), and the RNA nucleotide uridine monophosphate (UMP) as functions of impact energy. Full lines: present IAM-PCM calculations, long-dashed lines: present IAM-PCM calculations divided by the number of valence electrons (5), short-dashed lines: present IAM-PCM calculations divided by the number of bonding valence electrons (6) and further divided by ten for visibility, dotted lines: present IAM-PCM calculations divided by the IAM coefficients (7).

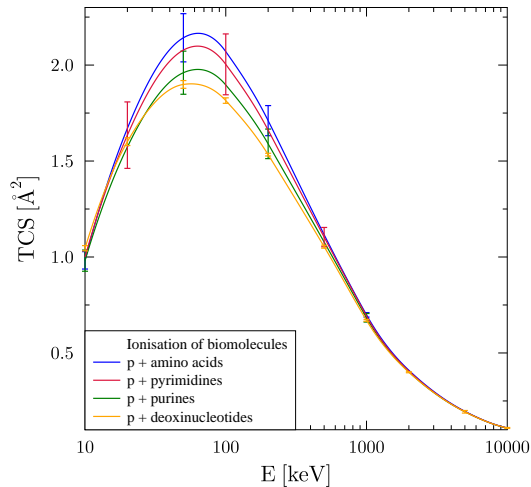


FIG. 8. Average (IAM-based) scaled net ionization cross sections using (7) for proton collisions with pyrimidines, purines, amino acids, and DNA nucleotides as functions of impact energy. The deviations of the actual results displayed in figure 7 from the averages are shown as error bars.

addition to the atomic net ionization cross sections obtained from the TC-BGM calculations displays Bethe-Born results in which the parameters A and B in the cross section formula

$$\sigma_{\text{Bethe}}(E) = \frac{A \ln E}{E} + \frac{B}{E} \quad (8)$$

were determined by a fitting procedure using the Fano representation [22]. The agreement is excellent for impact energies above $E \approx 200$ keV. At lower energies, the TC-BGM cross sections are smaller than the Bethe-Born predictions, mostly because electron capture (which is described by the TC-BGM) gains importance and ultimately takes over as the dominant electron removal channel. One may argue that the occurrence of capture effectively decreases the projectile charge Q_P , thereby reducing the amount of direct ionization to the continuum, which in the Bethe-Born approximation is proportional to the square of Q_P [40]. This suggests the ansatz

$$\sigma^{\text{ion}}(E) = [Q_{P,\text{eff}}(E)]^2 \sigma_{\text{Bethe}}(E) \quad (9)$$

with an effective charge of the form

$$Q_{P,\text{eff}}(E) = 1 - a \exp(-\alpha E). \quad (10)$$

We note that similar parametrizations have been proposed in the past to model the electron loss from neutral projectiles (see [41] and references therein). The full circles in figure 6 show

TABLE I. Parameters α (in keV^{-1}) and a used in (10) to model the effective charges for the atomic targets hydrogen (H), carbon (C), nitrogen (N), oxygen (O), and phosphorus (P).

	H	C	N	O	P
α	0.030	0.033	0.024	0.021	0.040
a	1.10	0.94	0.91	0.87	1.00

the results obtained from equations (9) and (10) with the parameters listed in Table I. The agreement with the TC-BGM cross section curves is almost perfect. A similar parametrization should then work for biomolecular targets. However, in this case we found that the overlap effects taken into account in the IAM-PCM result in a flatter shape of the cross section curves compared to their atomic counterparts and the modified formula

$$\sigma_{\text{mol}}^{\text{ion}}(E) = [1 - a \exp(-\alpha\sqrt{E})]^2 \sigma_{\text{Bethe}}(E) \quad (11)$$

provides better fits. This is demonstrated for the nucleotides in figure 9. Formula (11) agrees with the orientation-averaged IAM-PCM calculations in the entire impact energy range from $E = 10 \text{ keV}$ to $E = 10 \text{ MeV}$ to within $\pm 3\%$.

VI. CONCLUDING REMARKS

We have used the IAM-PCM, introduced in recent work, to calculate proton-impact net ionization cross sections for a large class of biologically relevant molecules from $E = 10 \text{ keV}$ to $E = 10 \text{ MeV}$ impact energy. We have found overall good agreement with the limited experimental data available for pyrimidine, purine, THF, and TMP and have made predictions for a number of larger systems including amino acids and nucleotides. To our knowledge, the results reported for the latter are the first cross sections obtained from a parameter-free theoretical model. It is shown that they follow a scaling rule which is based on IAM-derived fractional coefficients and can be represented by a simple analytical formula to within 3% accuracy. Scaling prescriptions based on the number of (bonding) valence electrons which were advocated in previous works yield less conclusive results.

The IAM-PCM is based on a geometrical interpretation of a molecular total cross section as the combined area of overlapping circles which represent atomic cross sections. The latter are calculated from first principles using accurate atomic potentials and the nonperturbative

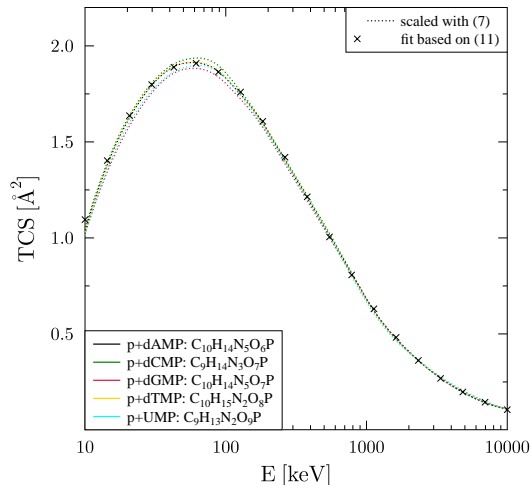


FIG. 9. IAM-based scaled net ionization cross sections using (7) for proton collisions with the DNA nucleotides deoxyadenosine monophosphate (dAMP), deoxycytidine monophosphate (dCMP), deoxyguanosine monophosphate (dGMP), deoxythymidine monophosphate (dTMP), and the RNA nucleotide uridine monophosphate (UMP) as functions of impact energy. Crosses: fit based on (11) using the parameters $A = 135.0 \text{ \AA}^2\text{keV}$, $B = -190.0 \text{ \AA}^2\text{keV}$, $a = 0.965$ and $\alpha = 0.102 \text{ keV}^{-1/2}$.

TC-BGM for orbital propagation. Once these cross sections have been computed, the IAM-PCM procedure to assemble the molecular cross section is computationally inexpensive and numerically accurate.

We envision that the method can be used to describe collisions involving long-chain molecules and polymers, such as peptides and large DNA sections, in terms of cross section calculations for (clusters of) amino acids and nucleotides. Further work in this direction is in progress. Future studies will also be concerned with the electron capture channel and with the extraction of charge-state-correlated multiple ionization data. The latter will be particularly relevant for collision systems involving multiply-charged projectile ions.

ACKNOWLEDGMENTS

This work was supported by the Natural Sciences and Engineering Research Council of Canada (NSERC). One of us (H. J. L.) would like to thank the Center for Scientific Computing, University of Frankfurt for making their High Performance Computing facilities

available.

-
- [1] G. Garcia Gómez-Tejedor and M. C. Fuss, eds., *Radiation Damage in Biomolecular Systems* (Springer, Dordrecht, 2012).
 - [2] P. Moretto-Capelle and A. Le Padellec, Phys. Rev. A **74**, 062705 (2006).
 - [3] J. Tabet, S. Eden, S. Feil, H. Abdoul-Carime, B. Farizon, M. Farizon, S. Ouaskit, and T. D. Märk, Phys. Rev. A **81**, 012711 (2010).
 - [4] J. Tabet, S. Eden, S. Feil, H. Abdoul-Carime, B. Farizon, M. Farizon, S. Ouaskit, and T. D. Märk, Phys. Rev. A **82**, 022703 (2010).
 - [5] Y. Iriki, Kikuchi Y., M. Imai, and Itoh A., Phys. Rev. A **84**, 032704 (2011).
 - [6] Y. Iriki, Kikuchi Y., M. Imai, and Itoh A., Phys. Rev. A **84**, 052719 (2011).
 - [7] A. Itoh, Y. Iriki, M. Imai, C. Champion, and R. D. Rivarola, Phys. Rev. A **88**, 052711 (2013).
 - [8] W. Wolff, H. Luna, L. Sigaud, A. C. Tavares, and E. C. Montenegro, J. Chem. Phys. **140**, 064309 (2014).
 - [9] B. Rudek, D. Bennett, M. U. Bug, M. Wang, W. Y. Baek, T. Buhr, G. Hilgers, C. Champion, and H. Rabus, J. Chem. Phys. **145**, 104301 (2016).
 - [10] M. C. Bacchus-Montabonel, Chem. Phys. Lett. **664**, 173 (2016).
 - [11] C. Covington, K. Hartig, A. Russakoff, R. Kulpins, and K. Varga, Phys. Rev. A **95**, 052701 (2017).
 - [12] E. S. Teixeira, K. Uppulury, A. J. Privett, C. Stopera, P. M. McLaurin, and J. A. Morales, Cancers **10**, 136 (2018).
 - [13] M. E. Rudd, Y. K. Kim, D. H. Madison, and J. W. Gallagher, Rev. Mod. Phys. **57**, 965 (1985).
 - [14] N. Stolterfoht, R. D. DuBois, and R. D. Rivarola, *Electron Emission in Heavy Ion-Atom Collisions* (Springer, Berlin, 1997).
 - [15] E. C. Montenegro, G. M. Sigaud, and R. D. DuBois, Phys. Rev. A **87**, 012706 (2013).
 - [16] C. Champion, H. Lekadir, M. E. Galassi, O. A. Fojón, R. D. Rivarola, and J. Hanssen, Phys. Med. Biol. **55**, 6053 (2010).
 - [17] S. Paredes, C. Illescas, and L. Méndez, Eur. Phys. J. D **69**, 178 (2015).
 - [18] M. E. Galassi, C. Champion, P. F. Weck, R. D. Rivarola, O. A. Fojón, and J. Hanssen, Phys. Med. Biol. **57**, 2081 (2012).

- [19] C. Champion, P. F. Weck, H. Lekadir, M. E. Galassi, O. A. Fojón, P. Abufager, R. D. Rivarola, and J. Hanssen, *Phys. Med. Biol.* **57**, 3039 (2012).
- [20] C. Champion, M. E. Galassi, P. F. Weck, S. Incerti, R. D. Rivarola, O. A. Fojón, J. Hanssen, Y. Iriki, and A. Itoh, *Nucl. Instrum. Methods Phys. Res. Sec. B* **314**, 66 (2013).
- [21] H. J. Lüdde, A. Achenbach, T. Kalkbrenner, H.-C. Jankowiak, and T. Kirchner, *Eur. Phys. J. D* **70**, 82 (2016).
- [22] H. J. Lüdde, M. Horbatsch, and T. Kirchner, *Eur. Phys. J. B* **91**, 99 (2018).
- [23] D. Young, *Computational Chemistry: A Practical Guide for Applying Techniques to Real World Problems* (Wiley Interscience, New York, 2001).
- [24] MolView: <http://molview.org> [Online; accessed 2019-01-05].
- [25] T. Kirchner, L. Gulyás, H. J. Lüdde, E. Engel, and R. M. Dreizler, *Phys. Rev. A* **58**, 2063 (1998).
- [26] M. Zapukhlyak, T. Kirchner, H. J. Lüdde, S. Knoop, R. Morgenstern, and R. Hoekstra, *J. Phys. B* **38**, 2353 (2005).
- [27] F. Blanco and G. García, *Phys. Lett. A* **317**, 458 (2003).
- [28] M. U. Bug, W. Y. Baek, H. Rabus, C. Villagrassa, S. Meylan, and A. B. Rosenfeld, *Radiat. Phys. Chem.* **130**, 459 (2017).
- [29] M. Lalande, M. Abdelmouleh, M. Ryszka, V. Vizcaino, J. Rangama, A. Méry, F. Durantel, T. Schlathölter, and J.-C. Pouilly, *Phys. Rev. A* **98**, 062701 (2018).
- [30] R. L. P. Adams, R. H. Burdon, A. M. Campbell, D. P. Leader, and R. M. S. Smellie, *The Biochemistry of the Nucleic Acids* (Chapman and Hall, New York, 1981).
- [31] B. Alberts, A. Johnson, J. Lewis, D. Morgan, M. Raff, K. Roberts, and P. Walter, *Molecular Biology of the Cell* (Garland Science, New York, 2015).
- [32] M. U. Bug, *Nanodosimetric particle track simulations in water and DNA media*, Ph.D. thesis, University of Wollongong (2014).
- [33] H. Lekadir, I. Abbas, C. Champion, O. Fojón, R. D. Rivarola, and J. Hanssen, *Phys. Rev. A* **79**, 062710 (2009).
- [34] L. Sarkadi, *Phys. Rev. A* **92**, 062704 (2015).
- [35] C. Dal Cappello, P. A. Hervieux, I. Charpentier, and F. Ruiz-Lopez, *Phys. Rev. A* **78**, 042702 (2008).
- [36] H. J. Lüdde, M. Horbatsch, and T. Kirchner, (2019), in preparation.

- [37] R. H. Petrucci, F. G. Herring, J. D. Madura, and C. Bissonnette, *General Chemistry: Principles and Modern Applications* (Pearson, Toronto, 2017).
- [38] M. B. Shah and H. B. Gilbody, *J. Phys. B* **14**, 2361 (1981).
- [39] M. B. Shah, D. S. Elliott, and H. B. Gilbody, *J. Phys. B* **20**, 2481 (1987).
- [40] M. Inokuti, *Rev. Mod. Phys.* **43**, 297 (1971).
- [41] J. L. Gervasoni and S. Cruz-Jiménez, *Radiat. Phys. Chem.* **48**, 433 (1996).

Appendix A: Net ionization cross sections

In this appendix we present tables with the orientation-averaged IAM-PCM net ionization cross sections for all systems studied in section IV.

TABLE II. Orientation-averaged IAM-PCM net ionization cross sections for proton collisions with pyrimidines (in \AA^2).

E [keV]	Barbituric acid	Cytosine	Orotic acid	Pyrimidine	Thymine	Uracil
	$\text{C}_4\text{H}_4\text{N}_2\text{O}_3$	$\text{C}_4\text{H}_5\text{N}_3\text{O}$	$\text{C}_5\text{H}_4\text{N}_2\text{O}_4$	$\text{C}_4\text{H}_4\text{N}_2$	$\text{C}_5\text{H}_6\text{N}_2\text{O}_2$	$\text{C}_4\text{H}_4\text{N}_2\text{O}_2$
10	9.62	9.34	11.19	7.67	10.62	8.92
20	15.62	15.42	17.60	12.66	17.41	14.83
50	20.12	19.44	22.60	15.98	21.93	18.90
100	19.59	18.75	22.14	15.05	21.17	18.23
200	16.50	15.49	18.64	12.11	17.63	15.13
500	10.95	10.28	12.64	7.96	11.72	9.99
1000	6.86	6.46	8.07	4.96	7.35	6.21
2000	4.03	3.76	4.82	2.87	4.26	3.65
5000	1.94	1.80	2.30	1.38	2.03	1.76
10000	1.08	1.02	1.32	0.77	1.14	0.98

TABLE III. Orientation-averaged IAM-PCM net ionization cross sections for proton collisions with purines (in \AA^2).

E [keV]	Adenine	Caffeine	Guanine	Purine	Theobromine	Uric Acid	Xanthine
	$\text{C}_5\text{H}_5\text{N}_5$	$\text{C}_8\text{H}_{10}\text{N}_4\text{O}_2$	$\text{C}_5\text{H}_5\text{N}_5\text{O}$	$\text{C}_5\text{H}_4\text{N}_4$	$\text{C}_7\text{H}_8\text{N}_4\text{O}_2$	$\text{C}_5\text{H}_4\text{N}_4\text{O}_3$	$\text{C}_5\text{H}_4\text{N}_4\text{O}_2$
10	11.32	16.80	12.04	10.36	14.86	12.13	11.40
20	18.53	26.78	19.70	16.55	23.77	19.47	18.00
50	22.96	32.82	24.52	20.61	29.42	24.63	22.64
100	22.17	31.56	23.68	19.67	28.49	24.11	22.03
200	18.41	26.52	19.91	16.32	23.94	20.32	18.53
500	12.40	18.04	13.33	10.96	16.18	13.94	12.68
1000	7.86	11.25	8.47	6.88	10.35	8.86	8.10
2000	4.58	6.66	4.96	4.07	6.03	5.20	4.78
5000	2.18	3.20	2.39	1.93	2.95	2.52	2.32
10000	1.23	1.82	1.33	1.12	1.62	1.40	1.28

TABLE IV. Orientation-averaged IAM-PCM net ionization cross sections for proton collisions with amino acids (in \AA^2).

E [keV]	Alanine	Asparagine	Glycine	Leucine	Proline	Threonine	Valine
	$\text{C}_3\text{H}_7\text{NO}_2$	$\text{C}_4\text{H}_8\text{N}_2\text{O}_3$	$\text{C}_2\text{H}_5\text{NO}_2$	$\text{C}_6\text{H}_{13}\text{NO}_2$	$\text{C}_5\text{H}_9\text{NO}_2$	$\text{C}_4\text{H}_9\text{NO}_3$	$\text{C}_5\text{H}_{11}\text{NO}_2$
10	7.66	10.34	5.99	12.59	10.39	9.85	10.64
20	13.20	17.51	10.66	20.85	17.17	16.78	18.04
50	17.22	22.67	14.17	26.18	21.58	21.44	22.69
100	16.60	22.01	13.77	25.14	20.75	20.88	21.83
200	13.56	18.38	11.18	20.86	17.28	17.28	18.17
500	8.76	12.08	7.14	13.72	11.43	11.32	11.86
1000	5.45	7.61	4.44	8.50	7.08	7.14	7.57
2000	3.19	4.45	2.57	5.08	4.18	4.17	4.40
5000	1.53	2.16	1.21	2.40	2.01	2.02	2.09
10000	0.86	1.19	0.68	1.35	1.12	1.14	1.18

TABLE V. Orientation-averaged IAM-PCM net ionization cross sections for proton collisions with the nucleotides deoxyadenosine monophosphate (dAMP), deoxycytidine monophosphate (dCMP), deoxyguanosine monophosphate (dGMP), deoxythymidine monophosphate (dTMP), uridine monophosphate (UMP) (in \AA^2).

E [keV]	dAMP	dCMP	dGMP	dTMP	UMP
	$\text{C}_{10}\text{H}_{14}\text{N}_5\text{O}_6$	$\text{C}_9\text{H}_{14}\text{N}_3\text{O}_7\text{P}$	$\text{C}_{10}\text{H}_{14}\text{N}_5\text{O}_7\text{P}$	$\text{C}_{10}\text{H}_{15}\text{N}_2\text{O}_8\text{P}$	$\text{C}_9\text{H}_{13}\text{N}_2\text{O}_9\text{P}$
10	27.01	25.27	27.53	26.03	25.11
20	41.75	38.86	42.22	40.61	39.15
50	49.63	46.22	50.68	48.22	46.69
100	47.63	44.63	48.72	46.43	45.30
200	40.34	37.35	41.34	39.16	38.13
500	27.55	25.73	28.27	26.89	26.13
1000	17.76	16.40	18.33	16.90	16.48
2000	10.64	9.75	10.92	10.20	9.97
5000	4.94	4.57	5.33	5.07	4.94
10000	2.82	2.62	2.92	2.69	2.63